



Mechanism of surrounding rock failure in impact stress and in-situ stress in circular tunnel

Jun Zhou · Guangming Zhao · Xiangrui Meng · Chunliang Dong · Yang Qiao · Meilu Yu

Received: 21 September 2023 / Accepted: 29 November 2023
© The Author(s) 2023

Abstract With depth increase of many mines, the damage of surrounding rock by high ground stress cannot be ignored under the blasting excavation method. In view of the strong disturbance of surrounding rock caused by dynamic excavation and unloading under high initial rock stress conditions, based on the elastic unloading theory, the analytical solution of dynamic excavation and unloading stress is given using the residue theorem and Laplace inverse transform. The stress field distribution under the coupling effect of blasting load and initial rock stress is described. By making a rock model and implementing biaxial loading using a drop hammer to simulate the impact load, radial cracks generated by the impact stress wave and circumferential cracks generated by unloading during excavation were captured, and the stress change curve during excavation was monitored. The monitoring curve and theoretical curve have consistency in trend. Under the coupling effect of blasting load and initial stress, surrounding rock will generate tensile stress and broken, and

the unloading effect of initial stress occurs after the blasting load, which causes tensile damage to the surrounding rock. The stress field curve plotted by the theory explains well the crack propagation caused by the coupling effect of blasting load and initial stress.

Highlights

- By applying the conditions of the residue theorem and utilizing the translational invariance of the Laplace transform, a dynamic analytical solution is obtained for circular tunnels in a uniform stress field.
- Through experimental methods, the sequence of dominant effects between impact stress and in-situ stress is discovered, with the observation of radial cracks appearing before circumferential cracks.
- The curve law of dynamic strain variation in the monitoring data are consistent with the patterns predicted by the analytical solution.

Keywords Blasting load · Initial stress · Unloading · Impact test · Rock failure

1 Introduction

As the human demand for natural resources continues to increase, surface resources of underground

J. Zhou · G. Zhao · X. Meng · C. Dong · M. Yu
State Key Laboratory of Deep Coal Mine Mining
Response and Disaster Prevention and Control, Anhui
University of Science and Technology, Huainan 232000,
China

Y. Qiao (✉)
Oulu Mining School, University of Oulu, 90014 Oulu,
Finland
e-mail: Yang.Qiao@oulu.fi

mines are being depleted, and underground mining is continuing to develop at deeper levels. Drill and blast methods are commonly used for excavation of tunnels. Blast excavation can cause dynamic effects, leading to dynamic disasters such as rockburst and spalling (Cai 2008; Gong et al. 2023). In view of the new mechanical characteristics of deep rock excavation, the unloading mechanism and the dynamic adjustment mechanism during excavation are discussed through dynamic theory study and design experiment, which can play a practical reference role in the stability control of surrounding rock.

Based on the elastic transient wave theory, (Liu et al. 2022; Li et al. 2023; Zhang et al. 2023) discussed the dynamic unloading effect of rock mass during blasting excavation by studying the rock mass damage during the excavation of underground power plant chambers. (Hong et al. 2023) conducted dynamic tests and mechanism research on the layer cracking phenomenon that occurs in the strong unloading damage caused by tunnel excavation, and studied the unloading response characteristics of surrounding rock. Li et al. (2009) (Liu et al. 2022) assumed the displacement potential function, derived the integral-variational equations of the surrounding rock mass by using the Hamilton time-domain variational principle, and obtained the solution functions of the disturbed stress, strain and displacement of the tunnel surrounding rock mass by using Duhamel integration and matrix transformation. (Miklowitz 1960) solved a planar stress solution for circumferential tensile stresses generated by shock unloading mechanisms, using complex Laplace transforms and demonstrating the important simplification function of the inverse integral transform for related planar strain problems. Carter and Booker (1990) established and calculated the transient stress field through different numerical inversion methods based on a numerical calculation program. For the dynamic excavation of underground engineering rock masses, the rock mass is treated as an infinite elastic material. Yan et al. (2015) applied Miklowitz channel integral to study the dynamic unloading effect and failure mechanism of drilling and blasting excavation of circular tunnels under high ground stress. From the above theoretical research methods, the solution methods based on transient wave theory mainly focus on the application of circumferential integral and residue theorems. Among them, the calculation process of the circumferential

integral is too difficult and complicated, which is not conducive to popularization and application in the study of dynamic unloading theory. It is much easier to apply the residue theorem to find the singularities of the function in the frequency domain, and then solve the residue of the function at these singularities. Xiao et al. (2013) established a mechanical model for excavation unloading of circular tunnels and studied the distribution laws of radial and tangential initial stresses based on elastic dynamics and elastoplastic theory. Yan et al. (2012) studied the stress field changes under different forms of unloading equations and under geological stress conditions, established numerical simulations of hydroelectric station chambers, and analyzed the vibration magnitude under the conditions of geological stress unloading. Yi et al. (2016, 2018) analyzed the dynamic excavation coupling effect of explosive load and geological stress, established numerical simulations, and analyzed the effects on crack propagation under different lateral pressure coefficient conditions.

Model experiments are one of the main research methods to study rock failure. These experiments mainly focus on studying the mechanical properties of rocks under static and dynamic loading and unloading conditions, using rock specimen as the object of study. The static and dynamic characteristics of rocks and the energy evolution laws of loading and unloading have been extensively researched (Kwasniewski et al. 2012; Liu et al. 2020). In recent years, with the development of true triaxial testing machines, the size of the test specimens has expanded from single cylindrical bodies to larger cubic or rectangular specimens. He Manchao (Li et al. 2023) studied rockburst phenomenon under single and double unloading conditions. Li X B (Kun et al. 2015) studied the cracking failure mechanism of surrounding rock plate through true triaxial unloading test. Zhao Guangming (Liu et al. 2023a; b) studied single-side unloading through true triaxial testing machine and concluded that the unloading rock would appear dilatant springback phenomenon. Feng et al. (2021) developed a true triaxial testing machine that can well complete real-time acoustic monitoring of hard rock tests. Gong Fengqiang (Si et al. 2022) studied the simulation of rock burst under the unloading condition inside the tunnel through true triaxial testing machine, and well reproduced the V-shaped groove in the tunnel wall. Su et al. (2023) conducted failure

morphological characteristics of rock and rockburst after different high temperature action in true triaxial testing machine, and discussed the occurrence mechanism of high temperature rockburst. Researchers such as Gu Jincan (Yuan et al. 2014) have developed a 3D physical simulation model test system to simulate the zonal failure of surrounding rock under excavation and unloading conditions. Dong et al. (2018) has studied the dynamic excavation and unloading effects of high-stress tunnels.

There are few researches on the mechanism of dynamic unloading, and the existing solutions are complicated (Miklowitz 1960; Yan et al. 2015), which need to be simplified. And in experiment, most of the tests now use small rock specimens, the rock has great limitations, so the unloading effect cannot be directly reflected. In this paper, considering the initial stress and blasting load, taking linear unloading as an example, based on the application conditions of the residue theorem, and by means of the Lagrangian inversion, the dynamic analytical solution of excavation unloading in circular roadway under uniform stress field is obtained. And in experiment, use self-developed dynamic disturbance similar simulation testing device for tunnel surrounding rock was employed, which effectively monitored the rock mass failure throughout the entire dynamic excavation and unloading process and tested the stress-time variation curve throughout the process. An attempt was made to calculate the dynamic stress field curve under the coupling effect of explosive load and initial stress

without using a large number of inversion calculation methods, but rather using residue theorem combined with Laplace inverse transformation, which provided a reliable basis for further comprehensive study of the dynamic excavation and unloading mechanism by comparing the theoretical curve and the actual curve trend.

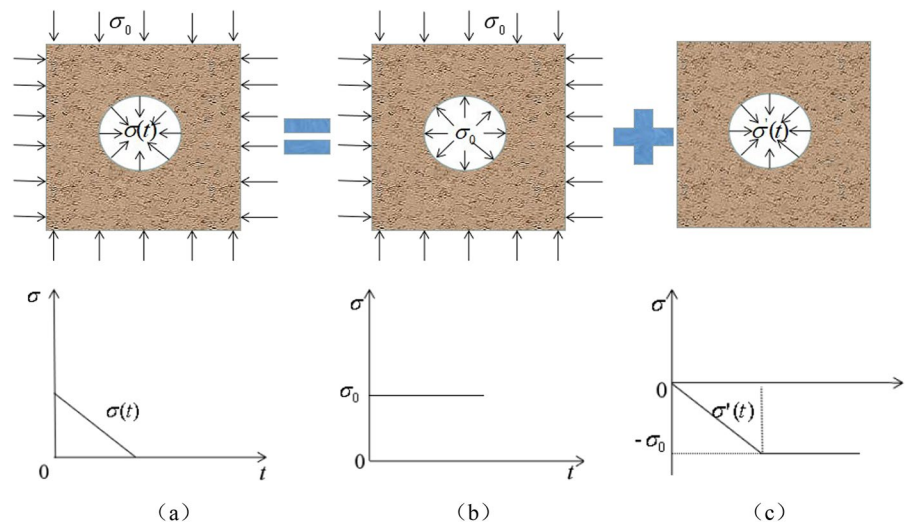
2 Transient unloading mechanism under couple of blast loading and in-situ stress

2.1 Transient unloading model under in-situ stress

When excavating a circular tunnel at a large depth in rock mass, the in-situ stress is uniformly distributed. To simplify the analysis, taking the excavation radius of a blast-formed tunnel as an example, the problem of uniform tunnel excavation is regarded as a plane strain problem, radial stress is σ_r , circular stress is σ_θ , and the stress at the excavation face is transiently released as a function $\sigma(t)$, as shown in Fig. 1a. The secondary stress field generated by this unloading process can be viewed as the superposition of static (Fig. 1b) and dynamic (Fig. 1c) problems, which can be easily obtained $\sigma_r = \sigma_\theta = \sigma_0$ according to the elastic stress solution of the thick-walled cylinder subjected to uniform pressure in an infinite rock mass.

Due to the symmetric characteristic, both the axial displacement and circumferential displacement are zero, and only the radial displacement occur. The problem of dynamic unloading of initial stress can

Fig. 1 Unloading mechanical model



be regarded as a boundary value problem of transient wave propagation in a cylindrical cavity subjected in a sudden uniform stress loading.

$$\frac{\partial^2 \Phi}{\partial r^2} + \frac{1}{r} \frac{\partial \Phi}{\partial r} = \frac{1}{c_p^2} \frac{\partial^2 \Phi}{\partial t^2} \tag{1}$$

$$\Phi(r, t) = 0, \frac{\partial \Phi(r, t)}{\partial t} = 0 \quad r \geq a \tag{2}$$

$$\sigma(r, t)|_{r=a} = \sigma(t) \quad t > 0 \tag{3}$$

$$\lim_{r \rightarrow \infty} \Phi(r, t) = 0 \quad t > 0 \tag{4}$$

In the equation, Φ is the displacement potential function, and the P-wave velocity in rock are

$$\begin{aligned} \Phi(r, t) &= \frac{4a^{\frac{5}{2}}c_p^2\sigma_0r^{-\frac{1}{2}}}{t_0} \left[\frac{1}{2\pi i} \int_{\alpha-i\infty}^{\alpha+i\infty} \frac{\exp(-st_0)}{s^2N(a, s)} \exp(st') ds - \frac{1}{2\pi i} \int_{\alpha-i\infty}^{\alpha+i\infty} \frac{1}{s^2N(a, s)} \exp(st') ds \right] \\ &= \frac{4a^{\frac{5}{2}}c_p^2\sigma_0r^{-\frac{1}{2}}}{t_0} \left[\frac{1}{2\pi i} \int_{\alpha-i\infty}^{\alpha+i\infty} \exp(-st_0)\bar{\phi}(s) \exp(st') ds - \frac{1}{2\pi i} \int_{\alpha-i\infty}^{\alpha+i\infty} \bar{\phi}(s) \exp(st') ds \right] \\ &= \frac{4a^{\frac{5}{2}}c_p^2\sigma_0r^{-\frac{1}{2}}}{t_0} \left\{ L^{-1} \left[\exp(-st_0)\bar{\phi}(s) \right] - L^{-1} \left[\bar{\phi}(s) \right] \right\} \end{aligned} \tag{10}$$

$c_p = 4500$ m/s, r is the radius and t is time, $t = 2.5$ ms. The stress solution is expressed in terms of Φ :

$$\sigma_r = (\lambda + 2\mu) \frac{\partial^2 \Phi}{\partial r^2} + \frac{\lambda}{r} \frac{\partial \Phi}{\partial r} \tag{5}$$

$$\sigma_\theta = \lambda \frac{\partial^2 \Phi}{\partial r^2} + \frac{(\lambda + 2\mu)}{r} \frac{\partial \Phi}{\partial r} \tag{6}$$

Performing a Laplace transform on Eqs. (1), (2), and (3), the solution of Φ in the time domain is obtained as:

$$\Phi(r, t) = \begin{cases} (A_1 \sin \alpha + B_1 \cos \alpha - A_2 \sin \beta - B_2 \cos \beta - D_1) r^{-1/2} & t' > t_0 \\ (-A_2 \sin \beta - B_2 \cos \beta - D_2 t' - H) r^{-1/2} & t_0 > t' > 0 \end{cases} \tag{13}$$

$$\Phi(r, t) = \frac{1}{2\pi i} \int_{\alpha-i\infty}^{\alpha+i\infty} \frac{4a^{\frac{5}{2}}c_p^2r^{-\frac{1}{2}}\bar{\sigma}(s)}{N(a, s)} \exp(st') ds \tag{7}$$

where $t' = t - (r - a)/c_p$.

The Eq. (7) contains the unloading function $\sigma(t)$, considering the initial stress unloading process as a linear unloading situation, $\sigma(t)$ can be written as:

$$\sigma(t) = \begin{cases} -\frac{\sigma_0}{t_0} t & 0 < t < t_0 \\ -\sigma_0 & t \geq t_0 \end{cases} \tag{8}$$

Its corresponding Laplace transform is:

$$\bar{\sigma}(s) = \frac{\sigma_0 [\exp(-st_0) - 1]}{s^2 t_0} \tag{9}$$

Substituting Eq. (9) into Eq. (7), as follows:

To solve the equation, we first transform the first term as follows:

$$L^{-1} \left[\exp(-st_0)\bar{\phi}(s) \right] = L^{-1} \left[\bar{\phi}(s) \right]_{t'-t_0} u(t' - t_0) \tag{11}$$

The second term can be transformed as follows:

$$L^{-1} \left[\bar{\phi}(s) \right] = L^{-1} \left[\bar{\phi}(s) \right]_t u(t') \tag{12}$$

Using the residue theorem to solve the inverse Laplace transform, the Eq. (10) is solved

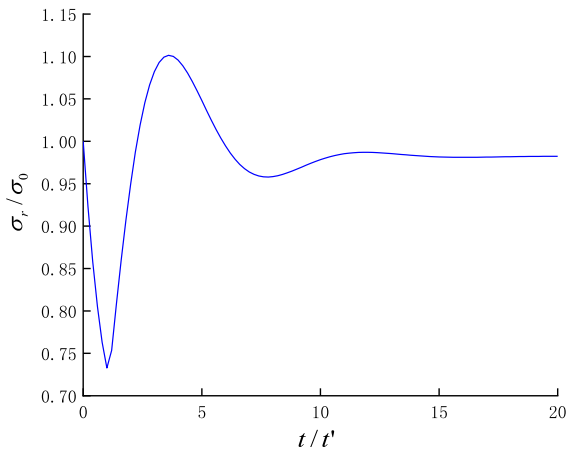


Fig. 2 Radial Stress Curve of In-situ Stress Unloading in $r=5a$

Table 1 Pressure-decay function

Function	Example
$P(t) = P_0 e^{-at}$	Sharpe (1942)
$P(t) = P_{VN}(e\gamma/n)^n H(t) t^n e^{-\gamma t}$	Blair (2007)
$P(t) = P_{jwl}(V(t))P_s(t)$	Cho and Kaneko (2004)
$P(t) = P_{VN}P_u(t)P_d(t)$	Trivino et al. (2009)

where $\alpha = \frac{Gc_p(t'-t_0)}{2(\lambda+2\mu)a}$, $\beta = \frac{Gc_p t'}{2(\lambda+2\mu)a}$,

$$A_1 = \frac{8a^{7/2}\sigma_0(4\mu^2-G^2)}{(\lambda+6\mu)^2 c_p G t_0} \exp\left[\frac{-\mu c_p(t'-t_0)}{(\lambda+2\mu)a}\right],$$

$$A_2 = \frac{8a^{7/2}\sigma_0(4\mu^2-G^2)}{(\lambda+6\mu)^2 c_p G t_0} \exp\left[\frac{-\mu c_p t'}{(\lambda+2\mu)a}\right],$$

$$B_1 = \frac{32a^{7/2}\sigma_0\mu}{(\lambda+6\mu)^2 c_p t_0} \exp\left[\frac{-\mu c_p(t'-t_0)}{(\lambda+2\mu)a}\right],$$

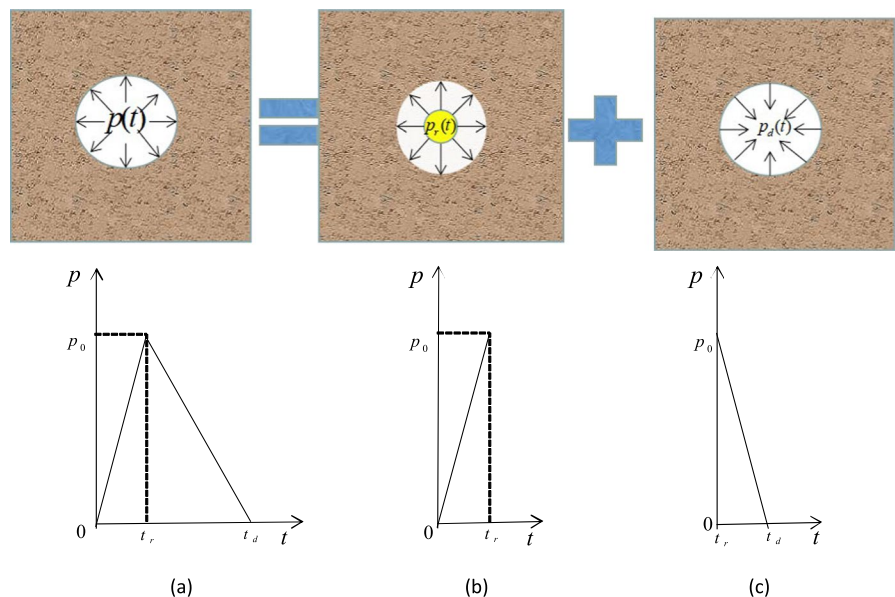
$$B_2 = \frac{32a^{7/2}\sigma_0\mu}{(\lambda+6\mu)^2 c_p t_0} \exp\left[\frac{-\mu c_p t'}{(\lambda+2\mu)a}\right], D_1 = \frac{4a^{5/2}\sigma_0}{(\lambda+6\mu)},$$

$$D_2 = D_1/t_0, H = \frac{-32a^{7/2}\sigma_0\mu}{(\lambda+6\mu)^2 c_p t_0}.$$

According to the residue theorem to solve the inverse Laplace transform of Eq. (10), and substituting the solution into Eq. (5), the dynamic stress field is obtained. Adding this solution to the static solution shown in Fig. 1b, the analytical solution for the excavation unloading problem in an infinite rock mass can be obtained. Figure 2 shows the radial stress as a function of time.

During the in-situ stress unloading process, the stress wave propagates at a velocity equivalent to the P-wave velocity in the medium. When the wave front arrives, the static stress state of the medium is disrupted, causing intense unloading disturbance in the vicinity of the unloading boundary. The dynamic stress exhibits rapid unloading rebound in the radial direction, showing the phenomenon of ‘super relaxation’.

Fig. 3 Blasting loading curve



2.2 Rock stress field induced by blast loading

Several pressure-decay functions have been used to model the pressure time history applied to the blasthole wall over the years (Table 1). The expression of load function is different, and the trend of function curve is the same. The variation curves of the load function over time are all represented by loading, and unloading is carried out after reaching the peak value. In order to simplify the calculation, the triangular wave explosion load model is adopted, as shown in Fig. 3a.

Blasting is a dynamic load formed in a short period of time, which produces a huge disturbance to the surrounding rock of the hole, and the crack spreads rapidly. The blast load function curve is like a triangle, and in order to simplified calculation, a triangular wave function is often used to represent the load function, as shown in Fig. 3.

Considering the stress field of surrounding rock under the condition of explosive loading, the unloading function $\sigma(t)$ in Eq. (8) can be described as Eq. (14), and $\sigma(t)$ can be written as:

$$p(t) = \begin{cases} p_0 \frac{t}{t_r} & 0 < t \leq t_r \\ p_0 \frac{t_d - t}{t_d - t_r} & t_r < t < t_d \\ 0 & t \geq t_d \end{cases} \quad (14)$$

Its corresponding Laplace transform is:

$$\bar{p}(s) = \frac{p_r + (sp_d - sp_{rd} + p_d) \exp(-st_d) + (sp_{rd} - sp_r t_r - sp_d t_r - p_r - p_d) \exp(-st_r)}{s^2} \quad (15)$$

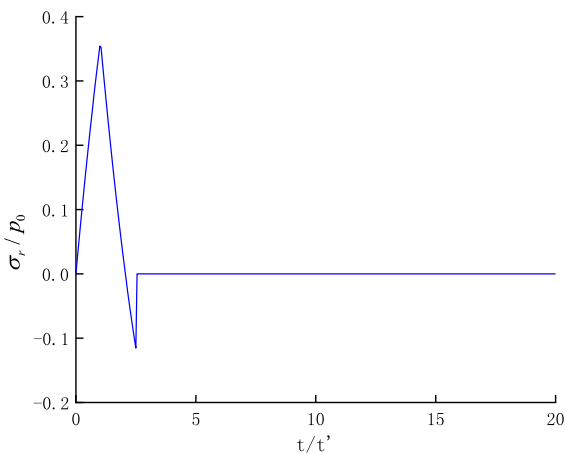


Fig. 4 Radial stress curve under explosive load in $r=5a$

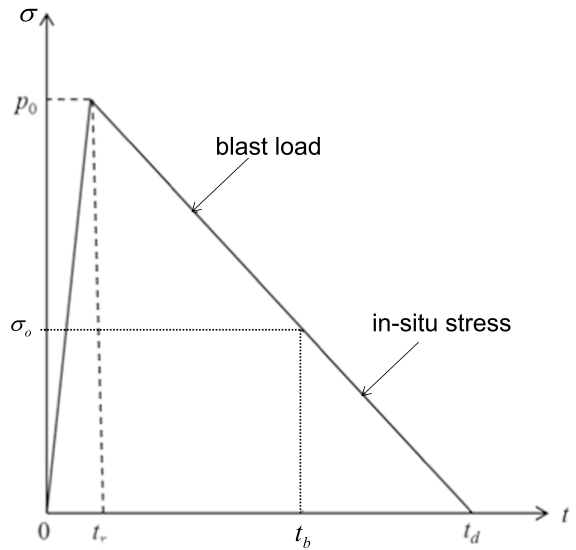


Fig. 5 The unloading process curve of in-situ stress and blast load

where $p_r = p_0/t_r, p_d = p_0/(t_d - t_r), p_{rd} = p_0 t_d / (t_d - t_r)$.

Substituting Eq. (15) into Eq. (7), and substituting the solution into Eq. (5). Assumed, $t_r = 1$ ms and $t_d = 2$. The radial stress field induced by blasting load was obtained and shown in Fig. 4.

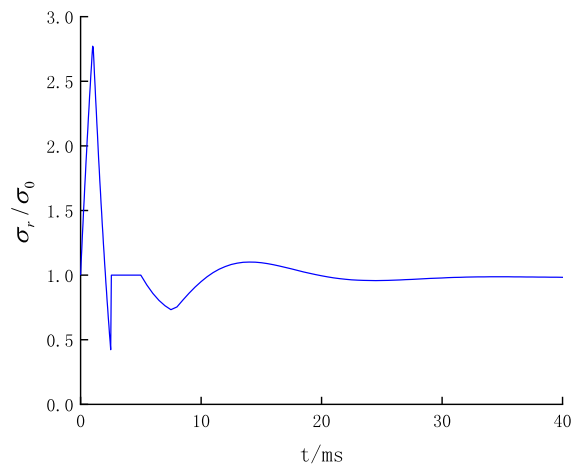


Fig. 6 Stress field under coupling of blast load and in-situ stress

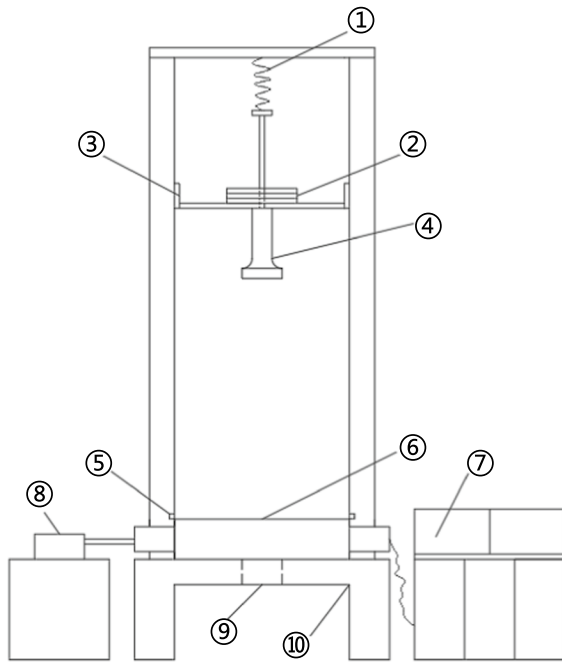


Fig. 7 Similar simulation test device for dynamic disturbance of roadway surrounding rock. ①-steel wire rope;②-weights;③-straightening frame;④-hammer head;⑤-laser;⑥-biaxial device;⑦-operate control;⑧-servo device;⑨-empty hole;⑩-fixed base

Figure 4 shows the radial stress-time curve induced by the explosion load. The ordinate represents the ratio of the dynamic stress peak to the peak pressure of the explosive load. Due to the strong impact characteristics of the explosion load, the radial stress rapidly rises to the compressive stress peak value in a very short time. As the explosion load is released, the radial stress in the rock mass around the excavated hole will change from compressive stress to tensile stress.

2.3 Rock stress field induced by blast loading and in-situ stress

For the blasting excavation of deep tunnel under ideal conditions, the surrounding rock must meet the stress continuity condition. During the unloading process, the stress attenuation is consistent with the reduction law of the ground stress when the load value drops to the in-situ stress. Therefore, the transient unloading curve of in-situ stress coincides with the curve of explosion load history after the beginning of unloading, and the in-situ stress on the excavation surface is the excavation load σ_0 , as shown in Fig. 5.

It is assumed that the impact time of the explosion load is 5 ms, and the in-situ stress occurs after the completion of the blast load. The dynamic stress field under the coupling of blast load and in-situ stress is shown in Fig. 6.

3 Dynamic excavation experiment

The self-developed equipment is used to simulate dynamic excavation, and similar proportion materials of rock mass are made. A drop hammer impacts the rock mass, resulting in a holes in impact load, and the same axial pressure is loaded on all sides to simulate rock mass underground stress and study the dynamic failure mechanism of rock mass.

3.1 Experimental design

The experimental system, as shown in Fig. 7, it is a self-developed dynamic simulation test device for rock-like mass. This test system can be used to study the failure mechanism of rock mass during

Table 2 Material parameters

Material	Density kg/m ³	Elasticity modulus/GPa	Poisson ratio	Tensile strength/MPa	Compressive strength/MPa	Wave velocity/m/s
Sandstone	2730	15.64	0.22	3.76	53.02	3608
Similar material	1700	0.45	0.21	0.11	1.33	1600

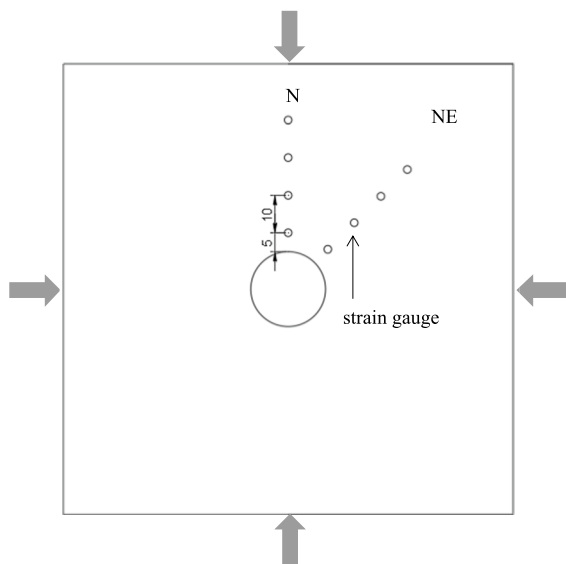


Fig. 8 Strain gauge set

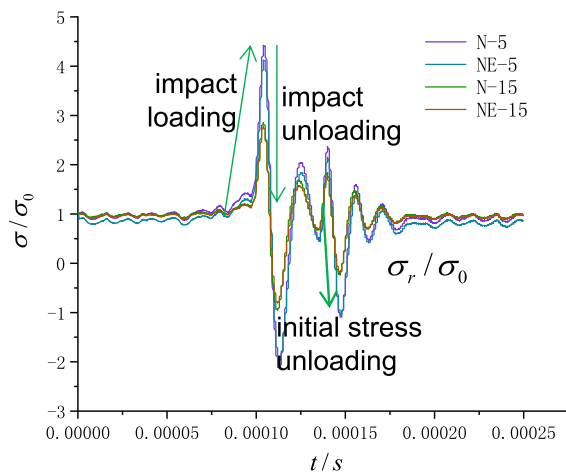


Fig. 9 Stress monitoring during excavation process

excavation, including the damage to the surrounding rock caused by excavation and the unloading effect.

The test was carried out using a test device where the sample was placed in a 6-load frame and the corresponding confining stress was applied. The ①-wire rope release is controlled by ②-control platforms, the ④-hammer free fall impacts the model inside the load frame, and the impacted model rushes out of the ⑤-empty hole.

According to Luling mine as the prototype, the rock mass belongs to typical argillaceous sandstone. In-situ raw rock is not easy to make, so similar simulation test is used. According to the material ratio sand, lime, gypsum is 4:3:2 with a mixer mix evenly. The 50×100 mm model specimen was made and its mechanical properties were tested. The material parameters are shown in Table 2.

Experiment have done 2 models of 120 cm×120 cm×30 cm, and applied the same axis compression in all directions. Strain gauges were set in the rock model, and were placed at distances of 5 cm, 15 cm, 25 cm, and 35 cm from the borehole in the N and NE directions. Data were obtained from the strain gauges located at distances of 5 cm and 15 cm from the hole, as follow Fig. 8.

3.2 Monitoring results

Four strain gauges monitored signal, and the test results are shown in Fig. 9. Only four monitored signal, such as N-5, N is the direction, 5 is 5 cm distance.

Strain gauges are embedded in the model rock mass to monitor the stress changes during the excavation process. The model has a certain initial stress, and the ratio of stress to initial stress ranges from 1 to the maximum positive value during loading, and from the maximum positive value to 1 during unloading. The stress-time curve during the dynamic excavation unloading under the coupling effect of initial stress and impact load is drawn, with compressive stress indicated as positive and tensile stress indicated as negative. The monitoring curve is shown in Fig. 10. The first detected is the shock stress wave signal with a large amplitude, which is of short duration and quickly decreases. The asymmetric stress wave signal, whose amplitude is lower than the impact stress wave signal, is generated by the axial loading stress. During the impact process, the entire unloading process takes place within 2.5 ms. The stress peak during the dynamic loading phase of the surrounding rock measuring point reaches 4.42 times the initial stress, and the stress peak during the dynamic unloading phase reaches 2.12 times the initial stress, while the stress peak during the initial stress unloading phase reaches 1.09 times the initial stress.

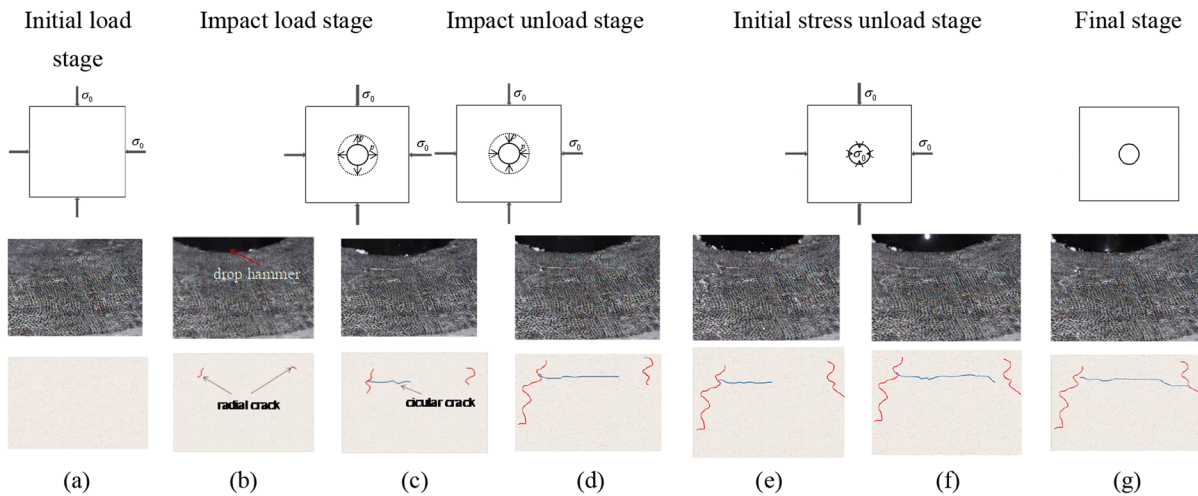


Fig. 10 Crack propagation process

3.3 Excavation and unloading process

The hammerhead diameter size is 20 cm, and the dynamic excavation device was used to excavate a circular tunnel with a diameter of 20 cm in the similar rock mass sample. A high-speed camera is arranged in the opposite direction of N to capture the change of surrounding rock cracks at the moment of punching.

Figure 10a shows the rock model before excavation, where the hammer has not yet fallen. In Fig. 10b, the black part represents the hammer head impacted by the hammer, which touches the rock mass and produces radial cracks around the excavated tunnel. The generation of cracks is caused

by the stress wave. Since the unloading surface has not yet formed, the strain energy within the rock mass has not been released. The starting toughness of the crack is provided by the impact energy. The dynamic impact releases the energy stored in the rock mass along the direction of the crack and causes crack propagation. The circumferential crack in Fig. 10c is generated by the coupling of dynamic impact stress and initial stress. The hammer impacts the rock mass model, and the radial stress wave produced by the impact causes the rock mass to crack. In this experiment, two radial cracks were formed, and the hammer continued to excavate along the axial direction while the cracks were

Fig. 11 Model failure after impact



expanding. The appearance of the free face caused a sharp adjustment of the original stress of the surrounding rock, and transient unloading occurred in the surrounding rock near the free face. The horizontal radial stress under unloading was approximately reduced to 0 MPa, and the loading direction also underwent stress adjustment. Due to the disappearance of the restraining effect of the surrounding rock on the tunnel in the direction of the free face caused by transient unloading, unloading stress waves were produced and had a tensile effect. Therefore, under the coupling of impact and initial stress unloading, the initial circumferential crack was generated from the weakest part of the surrounding rock (i.e., the radial crack) and propagated to adjacent radial cracks, forming circumferential cracks parallel to the tunnel. From energy perspective, the energy stored in the rock mass was rapidly released toward the free face. When the deformation of the rock exceeded the maximum strain it could withstand, the surrounding rock became unstable. Figure 10d shows the propagation of cracks. The energy of the shock wave weakens radially, and the strain energy of the surrounding rock continues to be released toward the free face. Both the radial and circumferential cracks continue to extend. In Fig. 10e, during the unloading process, the radial crack widens, and the model rebounds during the stress adjustment, causing the length of the circumferential crack to change compared to Fig. 10d. In

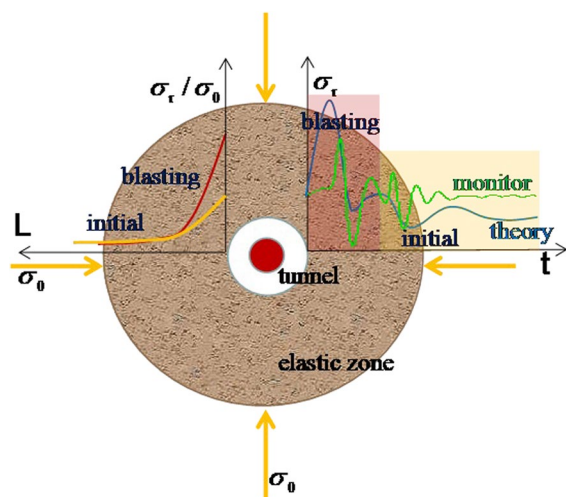


Fig. 12 Surrounding rock stress distribution

Fig. 10f, the crack further extends, and the circumferential crack forms a corner as it extends along the microcracks. In Fig. 10g, the circumferential and radial cracks penetrate and are perpendicular to each other at the junction of the circumferential and radial cracks.

Two models of the same material were made in the test, both of which had radial cracks and circumferential cracks. The impact results were shown in Fig. 11. Under the initial stress, the unloading produces tensile stress and significant circumferential cracks. The initiation direction of the circumferential crack is perpendicular to the radial crack, and the circumferential crack extends towards the adjacent radial crack. During the process of radial and circumferential crack propagation, small cracks in partially different directions are also produced.

4 Discussion

The jump point of strain signal is taken as the starting point and compared with the theoretical curve, as shown in Fig. 12 ($\sigma_r - t$). Theoretical calculations and actual measurement trends are consistent. The stress curve during the impact process was also monitored through similar simulation experiments, and the trend changes observed were consistent with the theoretical curve. In actual excavation processes, the explosive shock wave mainly forms a cavity and a fractured zone, excavating a certain area of the tunnel. Cracks appear in the elastic zone, shock stress wave effect the elastic zone. The cavity formed by the rock model impacted by the falling hammer represent excavated zone of the surrounding rock in actual excavation processes. The cracks by the rock model impacted by the falling hammer produced in the elastic zone.

The model size is more than 5 times the diameter, and the tunnel and surrounding rock are regarded as a plane strain problem. The external force acting on the plane is the original rock stress. The experiment used the same axis compression stress. After excavation forms a hole, the surrounding rock stress can be calculated using the thick-walled cylinder principle. The experimental hole is the excavation area, and the residual zone can be regarded as the elastic zone.

Figure 12 ($\sigma_r/\sigma_0 - L$) show the curve of the radial stress peak value generated by the explosion

load and the unloading condition of the initial stress, respectively, as the distance changes. As the distance increases, the stress peak value of the surrounding rock decreases. The stress peak value generated by the explosion load is much greater than that generated by the unloading of the initial stress.

Taking the example of a once-excavated deep tunnel with a full section, the explosive stress wave propagates from the excavation face into the surrounding rock, induced dynamic stress in the surrounding rock. The stress field in the surrounding rock and the dynamic stress field excited by the explosion load are superimposed in the corresponding time and space domains. As can be seen from the blue curve on the right coordinates, the stress time history curve induced by the dynamic load coupling shows that the disturbance of the explosive load to the surrounding rock occurs before the transient unloading of the initial stress, which is consistent with the facts. The explosive load breaks the rock mass and throws it away from the excavation face, causing the initial stress contained in the rock mass in the excavation area to be unloaded in an extremely short time. The stress peak value generated by the explosive load in the near-field of the borehole is large. At this time, the dynamic load effect dominates the disturbance of the surrounding rock, and the stress time history curve is significantly affected by the explosive stress wave, resulting in tensile stress in the surrounding rock, thereby forming a certain range of tensile fracture zone in the surrounding rock. Due to the high peak value and fast attenuation of the explosive stress wave, the coupled stress field in the near-field of the borehole is dominated by the explosive stress wave, while in the far-field, it is dominated by the unloading stress wave.

The monitor curve show that the impact stress wave disturbing the surrounding rock was first monitored, and then the unloading stress wave was monitored. This is consistent with the order of the disturbance of the surrounding rock by the dynamic load of the excavation in the field. The trend of the theoretical curve and the monitoring curve is quite consistent. The first to be generated is the compression stress wave. When the stress wave decreases and then to unload, a tensile stress wave will be generated. When most of the impact energy is dissipated and the impact force decreases in accordance with the initial

stress, unloading dominated by the initial stress will occur, resulting in a tensile stress. The experimental curve is consistent with the trend of the theoretical curve, indicating the reliability of the experiment and the applicability of this analytical method.

5 Conclusion

Deep rock masses are in a high and complex initial stress state. The change in stress field of the surrounding rock was solved and measured using theoretical models and experiments, and the monitored stress field change curve was compared with the calculated stress curve trend change, which showed consistency. The blasting excavation of deep rock masses in underground engineering under the process of explosion loading–unloading–ground stress unloading, which affects the surrounding rock fracture. According to the monitored images, the rock masses subjected to impact loads will first produce radial cracks, and after the appearance of boreholes, circumferential cracks will begin to form vertically from the radial cracks at a certain distance from the borehole under the effect of axial stress loading. Under the effect of unloading stress, the cracks will continue to expand until they reach the adjacent radial cracks and then stop.

Acknowledgements No.

Author contributions Conceptualization, GZ; methodology, YQ; formal analysis, CD; investigation, JZ; resources, JZ; data curation, JZ; writing—original draft preparation, JZ; writing—review and editing, JZ; visualization, MY; supervision, GZ; project administration, XM. All authors have read and agreed to the published version of the manuscript.

Funding Open Access funding provided by University of Oulu (including Oulu University Hospital). This work was supported by the National Natural Science Foundation of China (Grants no. 51974009) and China scholarship council CSC NO. 202208340047.

Availability of data and materials Data will be made available on request.

Declarations

Ethics approval and consent for publication The authors agree with the publication of the manuscript.

Competing interests The authors declare no competing interests.

Open Access This article is licensed under a Creative Commons Attribution 4.0 International License, which permits use, sharing, adaptation, distribution and reproduction in any medium or format, as long as you give appropriate credit to the original author(s) and the source, provide a link to the Creative Commons licence, and indicate if changes were made. The images or other third party material in this article are included in the article's Creative Commons licence, unless indicated otherwise in a credit line to the material. If material is not included in the article's Creative Commons licence and your intended use is not permitted by statutory regulation or exceeds the permitted use, you will need to obtain permission directly from the copyright holder. To view a copy of this licence, visit <http://creativecommons.org/licenses/by/4.0/>.

References

- Blair DP (2007) A comparison of Heelan and exact solutions for seismic radiation from a short cylindrical charge. *Geophysics* 72(2):E33–E41
- Cai M (2008) Influence of stress path on tunnel excavation response—numerical tool selection and modeling strategy. *Tunn Undergr Space Technol* 23(6):618–628
- Carter JP, Booker JR (1990) Sudden excavation of a long circular tunnel in elastic ground. *Int J Rock Mech Min Sci Geomech Abstr* 27(2):129–132
- Cho SH, Kaneko K (2004) Rock fragmentation control in blasting. *Mater Trans* 45(5):1722–1730
- Dong C, Zhao G, Lu X et al (2018) Similar simulation device for unloading effect of deep roadway excavation and its application. *J Mt Sci* 15(5):1115–1128
- Feng XT, Zhang J, Yang C et al (2021) A novel true triaxial test system for microwave-induced fracturing of hard rocks. *J Rock Mech Geotech Eng* 13(5):961–971
- Gong F, Wu W, Ren L (2023) Rockburst process and strength-weakening effect of the high-stress circular tunnel under internal unloading. *J Rock Mech Geotech Eng* 15(4):864–885
- Hong Z, Tao M, Wu C et al (2023) The spatial distribution of excavation damaged zone around underground roadways during blasting excavation. *Bull Eng Geol Environ* 82(4):155
- Kun DU, Li X, Li D et al (2015) Failure properties of rocks in true triaxial unloading compressive test. *Trans Nonferr Met Soc China* 25(2):571–581
- Kwasniewski M, Li X, Takahashi M (2012) True triaxial testing of rocks. Taylor and Francis, London, pp 35–49
- Li S, Qian Q, Zhang D et al (2009) Analysis of dynamic and fractured phenomena for excavation process of deep tunne. *Chin J Rock Mech Eng* 28(10):2104–2112
- Li J, Liu D, He M et al (2023) Experimental investigation of true triaxial unloading rockburst precursors based on critical slowing-down theory. *Bull Eng Geol Env* 82(3):65
- Liu C, Zhao G, Xu W et al (2020) Experimental investigation on failure process and spatio-temporal evolution of rockburst in granite with a prefabricated circular hole. *J Cent South Univ* 27(10):2930–2944
- Liu D, Lu W, Yang J et al (2022) Relationship between cracked-zone radius and dominant frequency of vibration in tunnel blasting. *Int J Rock Mech Min Sci* 160:105249
- Liu X, Yan P, Lu W et al (2023a) Investigation of dynamic crack formation mechanism based on a new crack dynamic driving model. *Comput Geotech* 159:105471
- Liu C, Zhao G, Xu W et al (2023b) Experimental study on failure characteristics of single-sided unloading rock under different intermediate principal stress conditions. *Int J Min Sci Technol* 33(3):275–287
- Miklowitz J (1960) Plane-stress unloading waves emanating from a suddenly punched hole in a stretched elastic plate. *J Appl Mech* 27(1):165
- Sharpe JA (1942) The production of elastic waves by explosion pressures; I, theory and empirical field observations. *Geophysics* 7(2):144–154
- Si X, Li X, Gong F et al (2022) Experimental investigation of failure process and characteristics in circular tunnels under different stress states and internal unloading conditions. *Int J Rock Mech Min Sci* 154:105116
- Su G, Ren H, Jiang J et al (2023) Experimental study on the characteristics of rockburst occurring at the working face during tunnel excavation. *Int J Rock Mech Min Sci* 164:105347
- Trivino LF, Mohanty B, Munjiza A (2009) Seismic radiation patterns from cylindrical explosive charges by analytical and combined finite-discrete element methods. In: Paper presented at the proceedings of the 9th international symposium on rock fragmentation by blasting, *Fragblast*
- Xiao J, Qiu S et al (2013) Dynamic and static analytical method and results analysis of unloading effect of circular tunnel excavation. *Chin J Rock Mech Eng* 32(12):2471–2480
- Yan P, Lu W, Chen M et al (2012) Dynamic response of rock mass induced by the transient release of in-situ stress. *Int J Rock Mech Min Sci* 53:129–141
- Yan P, Lu W, Chen M et al (2015) Contributions of in-situ stress transient redistribution to blasting excavation damage zone of deep tunnels. *Rock Mech Rock Eng* 48:715–726
- Yi C, Johansson D, Nyberg U et al (2016) Stress wave interaction between two adjacent blast holes. *Rock Mech Rock Eng* 49:1803–1812
- Yi C, Johansson D, Greberg J (2018) Effects of in-situ stresses on the fracturing of rock by blasting. *Comput Geotech* 104:321–330
- Yuan L, Xue J et al (2014) Model test on zonal fracture of deep surrounding rock. *J China Coal Soc* 39(06):987–993
- Zhang X, Yan P, Lu W et al (2023) Energy release and damage characteristics induced by fracture planes in face destress blasting. *Int J Impact Eng* 173:104485

Publisher's Note Springer Nature remains neutral with regard to jurisdictional claims in published maps and institutional affiliations.